PHYSICAL REVIEW A **84**, 033423 (2011)

Stabilization of circular Rydberg atoms by circularly polarized infrared laser fields

S. Askeland,[1,*] S. A. Sørngård,[1,†] I. Pilskog,[1,2] R. Nepstad,[1] and M. Førre[1,‡]
[1]*Department of Physics and Technology, University of Bergen, N-5007 Bergen, Norway*
[2]*Laboratoire de Chimie Physique - Matière et Rayonnement, Université Pierre et Marie Curie - CNRS (UMR 7614), F-75231 Paris Cedex 05, France*

(Received 31 August 2011; published 29 September 2011)

The ionization dynamics of circular Rydberg states in strong circularly polarized infrared (800 nm) laser fields is studied by means of numerical simulations with the time-dependent Schrödinger equation. We find that at certain intensities, related to the radius of the Rydberg states, atomic stabilization sets in, and the ionization probability decreases as the intensity is further increased. Moreover, there is a strong dependence of the ionization probability on the rotational direction of the applied laser field, which can be understood from a simple classical analogy.

DOI: 10.1103/PhysRevA.84.033423 PACS number(s): 32.80.Fb, 32.80.Rm, 32.80.Ee

I. INTRODUCTION

Photoionization of atoms and molecules by a single photon impact has been studied since the early days of quantum mechanics. For the simplest atomic system in nature, hydrogen, which has a binding energy of 13.6 eV, absorption of a single photon with an energy exceeding this value will induce direct breakup of the system. With increasing photon flux, additional photons can be absorbed, giving rise to multiphoton processes and above-threshold ionization (ATI) [1,2]. From perturbation theory calculations, a general increase in breakup probability with intensity of the imposed radiation field is expected. It therefore came as a big surprise to many when, more than 20 years ago, theoretical studies of atomic hydrogen in ultraintense, high-frequency laser fields showed some evidence of the complete opposite scenario, i.e., that the atom may eventually become more stable as the ionizing radiation gets stronger [3–11]. This rather counterintuitive phenomenon, called atomic stabilization, has since then been studied extensively; see, e.g., [12–15] and references therein. It has also been argued that atomic stabilization has a classical counterpart [16,17]. (See also [12] and references therein.) Very recently, the stabilization dynamics of helium in intense xuv laser pulses was investigated [18,19].

Primarily a high-frequency phenomenon, atomic stabilization is expected to be important at photon energies exceeding the binding energy of the system at hand and for very high intensities. In the case of the hydrogen atom, photon energies exceeding 13.6 eV and intensities on the order of 10^{16} W/cm^2 or more are required [9,20,21]. Up to present times, experimental confirmation of atomic stabilization in tightly bound atomic systems, such as neutral atoms in their ground state, has been obstructed due to lack of the laser technology required to produce the necessary conditions. The possibility of observing the phenomenon in excited atomic states was pointed out early [4,22–25], and the first experimental signature of atomic stabilization in low-lying Rydberg atoms was reported in 1993 [26,27] and later confirmed [28], irradiating $5g$ circular states in neon by intense ($\sim 10^{13}$–10^{14} W/cm^2) 620-nm linearly polarized laser pulses. The experimental findings are consistent with theoretical predictions [29–32].

In this work, we investigate atomic stabilization of circular Rydberg states in hydrogen exposed to short, intense circularly polarized laser pulses, using parameters well within reach of conventional Ti:sapphire lasers. The m quantum number is set equal to l for the initial state, so that the electron is "orbiting" the nucleus in a counterclockwise fashion. Furthermore, the field polarization vector is chosen to lie in the plane defined by the initial circular state. We show that stabilization occurs for a range of pulse durations and different initial states, and that the radius of the circular initial state determines at which intensities stabilization sets in. It is also shown that the polarization direction of the applied field has a significant impact on the ionization dynamics for lower lying Rydberg states. Specifically, at 800 nm the $5g$ circular state is orders of magnitude more likely to ionize with counterclockwise (co-rotating field) as opposed to clockwise (counter-rotating field) polarization at lower intensities, but both enter the stabilization regime at the same intensity. This difference disappears for more highly excited states, such as the $10l$ circular state. Classical ensemble calculations are performed to investigate the underlying mechanisms.

Atomic units, where m_e, $\hbar$, and e are scaled to unity, are used throughout unless stated otherwise.

II. METHOD

In this paper we study the ionization dynamics of hydrogen when the atom is excited to a low-lying circular Rydberg state and exposed to a rotating electric field. To that end we solve numerically the time-dependent Schrödinger equation (TDSE) in full dimensionality. The Hamiltonian of such a system, described in the frame of the velocity gauge and the dipole approximation, reads

$$H = \frac{\mathbf{p}^2}{2} - \frac{1}{r} + A_x(t)p_x + A_y(t)p_y. \quad (1)$$

Each component of the circularly polarized laser field, here represented by its vector potential, is modulated by a

*sigurd.askeland@ift.uib.no
†stian.sorngard@ift.uib.no
‡morten.forre@ift.uib.no

sine-squared carrier envelope,

$$A_j(t) = A_0 \sin^2\left(\frac{\pi t}{T}\right)\sin(\omega t + \phi_j), \tag{2}$$

where $A_0 = E_0/\omega$, E_0 is the peak amplitude of the electric field, ω is the laser frequency, and T is the total pulse duration. To make the field rotate in the xy plane, there is a phase difference between the two components. We define the field to be rotating clockwise (as seen from above) if $\phi_x = 0$ and $\phi_y = \pi/2$, and counterclockwise if the phases are interchanged.

The radial and angular ranks of the wave function are expanded in B splines and spherical harmonics, respectively,

$$\Psi(\mathbf{r},t) = \sum_{k,l,m} c_{klm}(t)\frac{B_k(r)}{r}Y_{lm}(\Omega). \tag{3}$$

The wave function, expressed as a vector of the expansion coefficients c_{klm}, is propagated forward in time using the unconditionally stable Cayley-Hamilton form of the time propagator

$$\left(\mathbf{S} + \frac{i\,\Delta t}{2}\mathbf{H}\right)\mathbf{c}(t + \Delta t) = \left(\mathbf{S} - \frac{i\,\Delta t}{2}\mathbf{H}\right)\mathbf{c}(t). \tag{4}$$

Here $\mathbf{H}$ is the Hamilton matrix of the TDSE and $\mathbf{S}$, with $S_{ij} = \int B_i(r)B_j(r)\,dr$, is the B-spline overlap matrix. The need for an overlap matrix stems from the fact that B-spline functions are not orthogonal.

This propagation scheme calls for solving a linear system of equations in each time step. The set is too large to be solved directly, and an iterative method must therefore be applied. The selected one is the so-called generalized minimum-residual method (GMRES) [33,34], a Krylov subspace method well suited for non-Hermitian systems of equations, which is the case in Eq. (4). As the system is rather stiff, a preconditioning of the matrix $(\mathbf{S} + i\,\Delta t/2\mathbf{H})$ is required to ensure a reasonable convergence of the GMRES iterations. For this purpose the incomplete LU factorization [34] is employed to provide an approximation $\mathbf{M}$ to the matrix. Thus we are in practice solving the system $\mathbf{M}^{-1}(\mathbf{S} + i\,\Delta t/2\mathbf{H})\mathbf{c} = \mathbf{M}^{-1}(\mathbf{S} - i\,\Delta t/2\mathbf{H})\mathbf{c}$, rather than the one in Eq. (4). Even so, a Krylov subspace spanned by up to 40 vectors are required to converge within a tolerance of 10^{-13} at the highest field intensities.

The large spatial extension of the Rydberg states requires large radial boxes when propagated in time. In our computations we use boxes with an upper bound between 600 and 2000 a.u., depending on the initial state and the electric field strength. We use a number of seventh-order B splines corresponding to one spline per unit length, and let them be equally distributed throughout the range. The angular basis is truncated at $l = 41$ in computations where $E_0 \leqslant 0.3$ a.u., and at $l = 63$ otherwise.

The ionization probability is found through projection of the wave function onto hydrogen bound states,

$$P_{\text{ion}} = 1 - |\langle\Psi(\mathbf{r},T)|\psi_{\text{bound}}\rangle|^2. \tag{5}$$

Another approach, i.e., projecting the final wave function onto continuum state wave functions (Coulomb waves), has also been applied to a selection of test cases in order to verify consistency with the bound state analysis.

All velocity gauge calculations were performed with the PYPROP framework [35], a PYTHON/C++ based software package for solving the TDSE; details may be found elsewhere [36,37]. Additional calculations were made with a split-operator approach using the acceleration form of the light-matter interaction (the Kramers-Henneberger frame of reference) [21,38], to independently check the reliability of our results.

III. RESULTS

The majority of the TDSE simulations were performed with a $5g$ ($m = 4$) initial state. This is a circular state, i.e., the probability density is roughly torus shaped. The torus is positioned in the xy plane symmetrically with respect to the z axis. We define the major radius of the torus to be equal to the expectation value of r, viz. 27.5 a.u. Our case differs from the scenario studied earlier [26–32] in that we apply (in-plane) circularly polarized pulses, with components in the x and y directions, instead of z polarized fields. Thus, the axial symmetry of the problem is broken, resulting in a strong m mixing. In addition, we model a Ti:sapphire laser pulse with a wavelength of 800 nm. For all initial states considered, the photon energy $\hbar\omega$ exceeds the binding energy E_i, viz. $\hbar\omega > E_i$, and atomic stabilization is expected to occur at high intensities [12]. The ionization and stabilization dynamics are studied for pulses of different durations and varying peak intensities.

In the following discussion the reader will notice that we continually refer to the term "excursion amplitude." By this we mean the spatial displacement of a classical free electron influenced by an electric field. This quantity, also known as the quiver amplitude, is given by $\alpha = E_0/\omega^2$.

At the considered wavelength, nondipole effects are expected to play a role when the intensity exceeds 10^{16} W/cm^2. As the majority of the calculations were performed at intensities significantly lower than this, nondipole effects were not expected to be important here. To further confirm this, additional calculations including nondipole terms were conducted [21,39]. Regarding relativistic effects, these should also be negligible, because the maximum quiver velocity ($v = E_0/\omega$) attained by the electron in our calculations is less than 9% of the speed of light.

We first consider the TDSE calculations for the $5g$ initial state; see the left panels in Fig. 1. These depict the ionization probabilities as a function of the peak intensity of the laser pulse, for a number of pulse durations, ranging from 4 to 12 optical cycles. In all cases, stabilization, i.e., a local maximum in the ionization probability, occurs for excursion amplitudes in the vicinity of $\langle r\rangle = 27.5$ a.u., indicated by a dashed vertical line in the figure. The probability density of the initial state is shown as a shaded shape at the bottom of the lower panel. With circularly polarized light, there are two field configuration options: the field either co-rotates or counter-rotates relative to the electronic probability current in the torus. The upper (left) panel in Fig. 1 depicts the results for the co-rotation scenario, while the lower panel shows the corresponding results for the counter-rotation case. There is a slight difference in the position of the stabilization threshold for the two cases: 21 a.u. for counter-rotation and 28 a.u. for co-rotation.

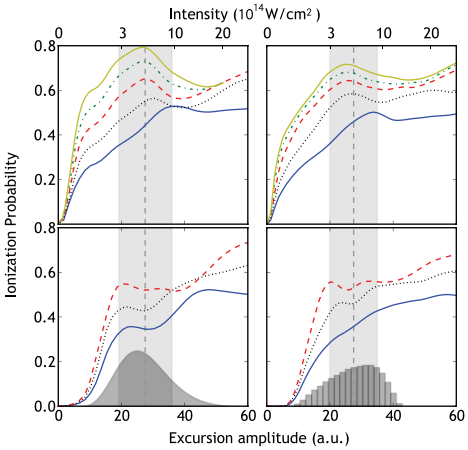

FIG. 1. (Color online) Ionization probability as function of excursion amplitude and laser intensity for the circular $5g$ ($m = 4$) state. The laser wavelength is 800 nm. The left panels are TDSE results, and the right panels are results from classical trajectory Monte Carlo (CTMC) calculations. For the upper panels a circular field that is co-rotating with respect to the electronic motion was used. The curves, from bottom up, represent laser pulses with 4, 6, 8, 10, and 12 optical cycles. The lower panels are the results for the corresponding counter-rotating case. Here, the curves, from bottom up, represent laser pulses with 4, 6, and 8 optical cycles. The shaded function in the bottom left panel is the shape of the radial probability distribution of the initial (quantum mechanical) state, and the histogram in the bottom right panel represents the distribution of initial radii for the electrons in the CTMC simulations. The dashed lines mark the radial expectation values $\langle r \rangle$ in the two cases, and the lighter shaded areas indicate the widths of the initial probability distributions, here taken to be the standard deviation.

When comparing the upper and lower (left) panels in Fig. 1, it is worth noting the different behavior at low intensities. While the curves for the co-rotation set out with a steep inclination, for the counter-rotation case they display a much more gradual increase. Quantum mechanically, the great difference in ionization yields between the co- and counter-rotation cases for lower field strengths is simply connected to a correspondingly great difference in their respective electric dipole couplings. For a circular state, the dipole selection rules for the absorption of one photon from the field are

$$\begin{aligned} \text{Counter-rot.: } \Delta m = -1, \quad & \text{Co-rot.: } \Delta m = +1, \\ \Delta l = \pm 1, \quad & \Delta l = +1. \end{aligned} \tag{6}$$

Thus, as long as one-photon absorption is the dominant ionization channel, the co-rotating field is more likely to ionize the system, simply because the relevant dipole couplings are about an order of magnitude larger (for the $n = 5$ circular state) than those relevant to the counter-rotating field. For more highly excited circular states, the difference between co- and counter-rotation is less pronounced, as can be seen in Fig. 2.

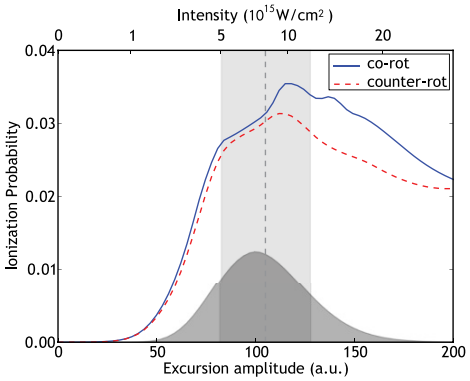

FIG. 2. (Color online) Ionization probability as function of excursion amplitude and laser intensity for the circular $10l$ ($m = 9$) state in circularly polarized electric fields with the wavelength 800 nm. The shaded function is the shape of the radial probability distribution of the initial state, and the dashed line marks its radial expectation value. The width of the torus, represented by the standard deviation of the radial distribution, is shown in a lighter shade of grey.

It is no coincidence that the value of the excursion amplitude at the point of stabilization coincides with the radius of the initial state probability density torus. When selecting the $10l$ ($m = 9$) state as the initial state (see Fig. 2), whose torus radius is 105 a.u., we get the stabilization threshold at 110–115 a.u., well within the "width" of the torus. Note that the co- and counter-rotating cases yield very similar results in this case, especially for the lower excursion amplitudes (field intensities), the reason being that the electron's (classical) "orbit" frequency is very low compared to the field frequency, making the difference between the co- and counter-rotating scenarios less important. We observe the same with a $7i$ ($m = 6$) initial state (not shown here), where again the stabilization threshold occurs at excursion amplitudes that approximately correspond to the torus radius, which in that case is 52.5 a.u. We made sure this connection also existed when using a different laser frequency, and if we used an in-plane linearly polarized laser field instead. Figure 3 shows the results for an x polarized laser pulse on a $5g$ ($m = 4$) initial state for pulses of 4, 6, and 8 optical cycles, and the results are, in fact, in qualitative agreement with the results in Fig. 1.

The observed close correlation between the torus radius $\langle r \rangle$ and the value of the excursion amplitude (electric field strength) at the stabilization threshold, has a simple intuitive explanation. During the action of an intense pulse, the electric field will drive the torus-shaped electron "cloud" around, while the heavy nucleus is nearly stationary (completely so in our model). When the excursion amplitude approaches the radius of the initial-state torus, the strong electric field pulls the densest part of the electron cloud into the nucleus. In the case of circularly polarized fields, the entire length of the torus may then be pulled through the "nuclear area," with the consequence that there is a high likelihood for the electron to interact strongly with the nucleus. Keeping in mind that interaction

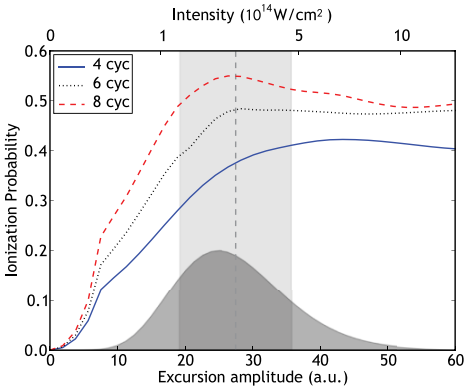

FIG. 3. (Color online) Ionization probability as function of excursion amplitude and laser intensity for the $5g$ ($m = 4$) state in a linearly polarized electric field along the x direction with the wavelength 800 nm. The shaded function is the shape of the radial probability distribution of the initial state, and the dashed line marks its radial expectation value. The width of the torus, represented by the standard deviation of the radial distribution, is shown in a lighter shade of grey.

with the nucleus is the catalyst for ionization, it should be of no surprise that the point of maximum ionization approximately coincides with the excursion of the initial (circular) state. For lower intensities and excursion amplitudes, the nucleus will remain inside the torus, causing less ionization. Similarly, at larger excursion amplitudes beyond the stabilization point, the torus is displaced to such an extent that it no longer intersects the nucleus, and less ionization occurs. However, since the central attractive force is no longer centered inside the torus, the latter will start to disperse, in effect ionizing. The balance of these two mechanisms qualitatively explains the local minima of the ionization probability after stabilization has occurred.

Looking at the probability density function during the pulse for the different orientations, see Fig. 4, we notice that in co-rotating scenarios, part of the electron cloud is quickly pulled in close to the nucleus. This does not happen to the same extent in the counter-rotating scenarios. Specifically, Fig. 4 shows the probability density in the xy plane for half a cycle of the pulse when this phenomenon can easily be observed. The figure shows the developments for the co- and counter-rotating cases side by side. The arrows indicate the direction and strength of the electric field. The force on the electron works in the opposite direction. Looking at the left panels in Fig. 4, showing the counter-rotating scheme, we see little action. For the co-rotating case, on the other hand, a sizable portion of the electron probability is pulled to the nucleus at an early stage, making a spiraling tail structure behind the nucleus.

The ionization dynamics of Rydberg atoms in circularly polarized fields has been studied before in terms of classical mechanics [40,41]. The classical approach may facilitate the interpretation of the results from the quantum-mechanical

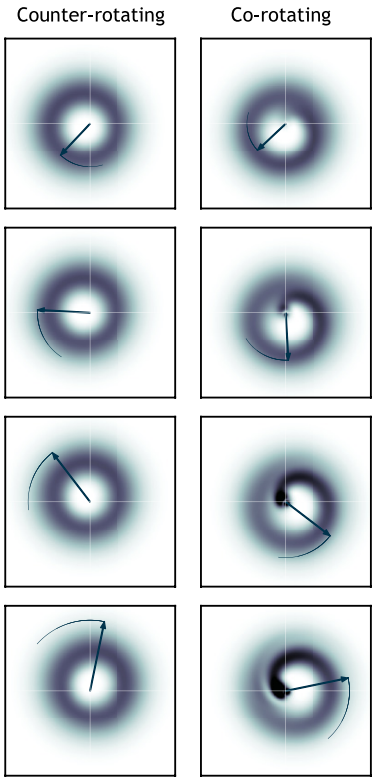

FIG. 4. (Color online) Snapshots of the probability density in the $z = 0$ plane, during half an optical cycle early in the laser pulse. The initial wave function is the circular $5g$ ($m = 4$) state, and the laser pulse contains four optical cycles. The peak intensity is 0.44×10^{14} W/cm^2, corresponding to an excursion amplitude of 8 a.u., but the figure depicts the probability density function when the intensity is in the range 0.1–0.4×10^{14} W/cm^2, or for an excursion amplitude of 3–7 a.u. The left panels show the clockwise rotation of the electric field, and the right panels show the co-rotation. The arrows illustrate the size and direction of the electric field. For the counter-rotating pulse, the ionization probability is 0.02, and the probability of staying in the initial state is 0.97. For the co-rotating pulse, the ionization probability is 0.24, and the probability of staying in the initial state is 0.71.

calculations, and provide further insight into the underlying physical mechanisms [40,41]. We therefore made supporting calculations using the classical trajectory Monte Carlo (CTMC) method [42,43]. Solving the Newtonian equations of motion for a large number (~30 000) of individual electron trajectories, corresponding to different initial conditions picked at random from a microcanonical ensemble [44–46], a classical estimate for the ionization probability P_{ion} is obtained

simply by taking the ratio between the number of trajectories corresponding to a free electron after the pulse and the total number of trajectories. To mimic the initial circular quantum state, only orbits fulfilling the constraint $(m - 1/2)\hbar < L_z < (m + 1/2)\hbar$, $m = l = n - 1$ being the quantum numbers of the hydrogenic circular state and L_z the z component of the angular momentum, were selected.

The results of the classical calculations are shown in the right panels in Fig. 1. Comparing left and right panels, i.e., the quantum and classical results, respectively, the similarity is striking. The agreement could be seen as a manifestation of Bohr's correspondence principle [47]. In particular, the stabilization phenomenon is clearly seen to have a classical counterpart [12,16,17]. The classical ensemble calculations further support the close relationship between the radius of the initial state (distribution) and the point (field excursion amplitude) at which stabilization sets in.

As is apparent from the CTMC results in Fig. 1, the classical approach is well suited for these stabilization simulations. It stands to reason that the different behavior for low intensities should have a classical explanation as well as the quantum-mechanical explanation given above. This may also give us a more intuitive feel for the mechanisms involved. First we adopt the CTMC view of the initial state, that of an ensemble of independent electrons orbiting the nucleus. All the electrons will orbit in a counterclockwise fashion, with approximately the same angular momentum, but varying degree of eccentricity. The electric field, when it is turned on, rotates much ($\sim \times 9$) faster than the electrons orbit the nucleus. The perturbations from the field drive the electrons into trajectories with a "telephone cord" appearance, in particular for higher field strengths. Regardless of rotational direction, the field will always alternately accelerate and decelerate the electron. This, however, is where the difference between co- and counter-rotation comes in. The periods of acceleration and deceleration will be longer in the co-rotating case than in the counter-rotating case, because the field and the electron are rotating in the same direction in the former case. The closer the frequency of the laser field is to the electron's rotation frequency, the longer the periods. For electrons in sufficiently eccentric orbits that pass close to the nucleus when the field is approximately aligned with the velocity of the electron, a large transfer of energy may occur in the co-rotating case. The eccentricity of the orbit is here crucial for the ionization to take place, since the instantaneous electronic rotation frequency should match the field frequency when the electron is closest to the nucleus. This field-assisted "slingshot maneuver" scenario [48,49] is illustrated in Fig. 5, where a single ionizing trajectory is shown, together with energy and angular frequency as a function of time. Here, the electron clearly receives two "kicks" when passing close to the nucleus, before entering an open, ionizing orbit. Although for the sake of simplicity, only a single classical trajectory is shown in the figure, we would like to emphasize that, in the limit of weak fields, all ionizing orbits will indeed exhibit a very similar behavior to the one depicted in Fig. 5. As such, the chosen example contains all essential features of the ionization dynamics in the limit of weak fields. In the counter-rotating case the slingshot effect becomes much less efficient, simply due to the counter-rotating fashion of the field, effectively causing less ionization. This explains the great difference in the ionization yields between the co- and counter-rotation cases in Fig. 1.

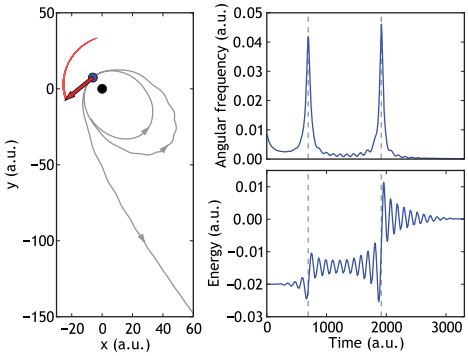

FIG. 5. (Color online) Left panel: The trajectory of a classical electron in an elliptical orbit being kicked out when closest to the nucleus (black dot). The red arrow indicates the direction of the force from the field acting on the electron (blue dot) at the very moment when the ionization takes place. Upper right panel: The angular frequency of the electron, relative to the origin, as function of time. Lower right panel: The energy of the electron as function of time. The two times the distance between electron and nucleus is minimized are marked by vertical dashed lines in the right panels. For the sake of illustration, the pulse applied in this figure is somewhat longer (30 cycles) than the pulses used throughout. The peak intensity is 1.08×10^{11} W/cm^2.

IV. CONCLUSION

By means of quantum simulations with the time-dependent Schrödinger equation supported by classical simulations using the classical trajectory Monte Carlo method, the ionization and stabilization dynamics of circular Rydberg states in hydrogen, subjected to circularly polarized 800-nm (Ti:sapphire) laser pulses, have been studied under experimentally realistic conditions. It is shown that at certain intensities, intimately related to the radius of the initial Rydberg states, atomic stabilization sets in. Both co- and counter-rotating fields with respect to the direction in which the electron orbits the nucleus were considered, and great differences in the corresponding ionization yields were identified, in particular for the lower-lying Rydberg states, but both enter the stabilization regime at similar intensities. These differences were reproduced in classical calculations, providing further insight into the underlying ionization mechanisms.

ACKNOWLEDGMENTS

This project was supported by the Bergen Research Foundation (Norway), and the computations were performed on the Cray XT4 (Hexagon) supercomputer at Parallab, University of Bergen (Norway). CPU hours were provided by the Norwegian Metacenter for Computational Science (NOTUR).

[1] P. Agostini, F. Fabre, G. Mainfray, G. Petite, and N. K. Rahman, Phys. Rev. Lett. **42**, 1127 (1979).
[2] W. Becker, F. Grasbon, R. Kopold, D. Milosevic, G. Paulus, and H. Walther, in *Advances In Atomic, Molecular, and Optical Physics*, Vol. 48, edited by B. Bederson and H. Walther (Academic, New York, 2002), p. 35.
[3] M. Pont, N. R. Walet, M. Gavrila, and C. W. McCurdy, Phys. Rev. Lett. **61**, 939 (1988).
[4] M. V. Fedorov and A. M. Movsesian, J. Phys. B **21**, L155 (1988).
[5] K. C. Kulander, K. J. Schafer, and J. L. Krause, Phys. Rev. Lett. **66**, 2601 (1991).
[6] K. Burnett, P. L. Knight, B. R. M. Piraux, and V. C. Reed, Phys. Rev. Lett. **66**, 301 (1991).
[7] M. Pont and M. Gavrila, Phys. Rev. Lett. **65**, 2362 (1990).
[8] Q. Su, J. H. Eberly, and J. Javanainen, Phys. Rev. Lett. **64**, 862 (1990).
[9] J. H. Eberly and K. C. Kulander, Science **262**, 1229 (1993).
[10] S. Geltman, J. Phys. B **27**, 257 (1994).
[11] S. Geltman, Chem. Phys. Lett. **237**, 286 (1995).
[12] M. Gavrila, J. Phys. B **35**, R147 (2002).
[13] A. M. Popov, O. V. Tikhonova, and E. A. Volkova, J. Phys. B **36**, R125 (2003).
[14] K. Yamanouchi, S. L. Chin, P. Agostini, G. Ferrante, and M. Fedorov, in *Progress in Ultrafast Intense Laser Science I*, Springer Series in Chemical Physics Vol. 84, (Springer, Berlin, 2006), p. 1.
[15] M. Boca, H. G. Muller, and M. Gavrila, J. Phys. B **37**, 147 (2004).
[16] J. Grochmalicki, M. Lewenstein, and K. Rzaewski, Phys. Rev. Lett. **66**, 1038 (1991).
[17] R. Grobe and C. K. Law, Phys. Rev. A **44**, R4114 (1991).
[18] T. Birkeland, R. Nepstad, and M. Førre, Phys. Rev. Lett. **104**, 163002 (2010).
[19] S. A. Sørngård, S. Askeland, R. Nepstad, and M. Førre, Phys. Rev. A **83**, 033414 (2011).
[20] M. Dondera, H. G. Muller, and M. Gavrila, Phys. Rev. A **65**, 031405(R) (2002).
[21] M. Førre, S. Selstø, J. P. Hansen, and L. B. Madsen, Phys. Rev. Lett. **95**, 043601 (2005).
[22] M. Pont and R. Shakeshaft, Phys. Rev. A **44**, R4110 (1991).
[23] R. J. Vos and M. Gavrila, Phys. Rev. Lett. **68**, 170 (1992).
[24] R. M. Potvliege and P. H. G. Smith, Phys. Rev. A **48**, R46 (1993).
[25] M. V. Fedorov, Laser Phys. **3**, 219 (1993).
[26] M. P. de Boer, J. H. Hoogenraad, R. B. Vrijen, L. D. Noordam, and H. G. Muller, Phys. Rev. Lett. **71**, 3263 (1993).
[27] M. P. de Boer, J. H. Hoogenraad, R. B. Vrijen, R. C. Constantinescu, L. D. Noordam, and H. G. Muller, Phys. Rev. A **50**, 4085 (1994).
[28] N. J. van Druten, R. C. Constantinescu, J. M. Schins, H. Nieuwenhuize, and H. G. Muller, Phys. Rev. A **55**, 622 (1997).
[29] B. Piraux and R. M. Potvliege, Phys. Rev. A **57**, 5009 (1998).
[30] A. M. Popov, O. V. Tikhonova, and E. A. Volkova, Laser Phys. **9**, 1053 (1999).
[31] A. M. Popov, O. V. Tikhonova, and E. A. Volkova, Laser Phys. **10**, 779 (2000).
[32] E. A. Volkova, A. M. Popov, and O. V. Tikhonova, J. Exp. Theor. Phys. **89**, 1045 (1999).
[33] Y. Saad and M. H. Schultz, J. Sci. Stat. Comput. **7**, 856 (1986).
[34] Y. Saad, *Iterative Methods for Sparse Linear Systems* (SIAM, Philadelphia, 2003).
[35] T. Birkeland and R. Nepstad, PYPROP, [http://pyprop.googlecode.com].
[36] T. Birkeland, Ph.D. thesis, University of Bergen, 2009.
[37] R. Nepstad, T. Birkeland, and M. Førre, Phys. Rev. A **81**, 063402 (2010).
[38] J. P. Hansen, T. Sørevik, and L. B. Madsen, Phys. Rev. A **68**, 031401 (2003).
[39] M. Førre, Phys. Rev. A **74**, 065401 (2006).
[40] D. Farrelly and T. Uzer, Phys. Rev. Lett. **74**, 1720 (1995).
[41] T. Uzer, E. Lee, and D. Farrelly, Phys. Rev. A **58**, 4761 (1998).
[42] R. Abrines and I. C. Percival, Proc. Phys. Soc. London **88**, 861 (1966).
[43] R. Abrines and I. C. Percival, Proc. Phys. Soc. London **88**, 873 (1966).
[44] C. O. Reinhold and C. A. Falcón, Phys. Rev. A **33**, 3859 (1986).
[45] J. P. Hansen, J. Lu, L. B. Madsen, and H. M. Nilsen, Phys. Rev. A **64**, 033418 (2001).
[46] H. M. Nilsen, L. B. Madsen, and J. P. Hansen, Phys. Rev. A **66**, 025402 (2002).
[47] N. Bohr, Z. Phys. **2**, 423 (1920).
[48] A. F. B. A. Prado, J. Guid. Control Dyn. **19**, 1142 (1996).
[49] U. Saalmann and J. M. Rost, Phys. Rev. Lett. **100**, 133006 (2008).